PCCP

PAPER

View Article Online
View Journal | View Issue

Open Access Article. Published on 08 February 2024. Downloaded on 1/11/2026 3:15:51 AM.
This article is licensed under a Creative Commons Attribution 3.0 Unported Licence.

Check for updates

Cite this: *Phys. Chem. Chem. Phys.*, 2024, **26**, 9197

Electron stimulated desorption from condensed benzene

L. Álvarez,[a] A. D. Bass,[b] A. I. Lozano,[acd] A. García-Abenza,[ae] P. Limão-Vieira,[c] L. Sanche[b] and G. García*[af]

Received 26th December 2023,
Accepted 7th February 2024

DOI: 10.1039/d3cp06289a

rsc.li/pccp

The electron induced dissociation of condensed benzene (C_6H_6) in thin films deposited on a Pt substrate is investigated by electron stimulated desorption (ESD) of anions and cations. The desorbed yields are recorded as a function of incident electron energy in the range of 10 to 950 eV for a fixed film thickness of 2 monolayers (ML) and for a fixed energy of 950 eV, as well as a function of film thickness from 0.5 to 8 monolayers (ML) for anions, and from 0.5 to 12ML for cations. Both energy and thickness dependencies are discussed in terms of the three main mechanisms yielding positively and/or negatively charged fragments: dissociative electron attachment (DEA), dipolar dissociation (DD) and dissociative ionization (DI) processes. At the probed energies, DD is the major mechanism, while DEA is predominantly induced by secondary electrons from the Pt substrate. Desorption of the parent positive ion is strongly suppressed. Similar qualitative behaviours are observed for the energy dependence of both anion and cation ESD yields, while some discrepancies exist in the thickness dependence, including a very significant systematic magnitude difference found between such ions formation. An estimation of the effective DD cross-section including the desorption probability is obtained. Feasible mechanisms behind the observed energy and thickness dependences for anion and cation yields are proposed. These results highlight the need for further investigations to better understand the underlying processes of electron induced dissociation in condensed matter.

Introduction

The study of radiation transport through matter has been a very relevant and active field of research for decades due to both its fundamental character and its pertinence to practical applications such as radiobiology, radiotherapy and radiation induced chemistry. The need to better understand the physical processes involved when radiation interacts with matter and the related induced local chemistry, the interactions of photons, electrons and ions with a wide variety of atoms and molecules have been intensively studied.

With respect to electrons, most studies have been focused on electronic collisions with gas-phase atomic and molecular targets. However, for many technological and even biological applications, a detailed knowledge of the underlying mechanisms governing the transport of electrons through condensed matter is needed. Accurate simulation of radiation damage to biological tissue is one of the most relevant of these.[1] The physical characteristics of tissue include much higher densities than gas-phase targets, implying a correspondingly stronger and more complex influence of the surrounding environment on electron-molecule interactions. Hence, as significant differences between electron scattering from gaseous and condensed molecules are anticipated, complementary approaches are required to account for the effects of condensation, which are highly relevant to the aforementioned applications. Within this framework, substantial efforts have been made in the investigation of electron interactions with thin biomolecular films.[1] During such work, electron stimulated desorption (ESD) measurements have been shown to be a very effective technique to understand the effects of low energy electron-induced fragmentation processes in condensed molecules.

The molecular target of the present study, benzene, is the smallest and simplest aromatic hydrocarbon and a representative non-polar molecule with an extremely large molecular polarizability. It is also considered a prototype for many complex molecules present in living tissues, *i.e.*, DNA and RNA pyrimidine bases, and molecular analogs. From a technological point of view, it is a relevant chemical compound in the petroleum industry,[2] as

[a] *Fundamental Physics Institute, Consejo Superior de Investigaciones Científicas, Serrano 113-bis, Madrid 28006, Spain. E-mail: g.garcia@csic.es*
[b] *Department of Nuclear Medicine and Radiobiology, Faculty of Medicine and Health Sciences, University of Sherbrooke, Québec, Canada*
[c] *Laboratório de Colisões Atómicas e Moleculares, CEFITEC, Departamento de Física, NOVA School of Science and Technology, Universidade NOVA de Lisboa, Caparica 2829-516, Portugal*
[d] *Institut de Recherche en Astrophysique et Planétologie (IRAP), Université Toulouse III - Paul Sabatier, 9 Avenue du Colonel Roche, Toulouse 31028, France*
[e] *Spanish Meteorological Agency (AEMET), Murcia, Spain*
[f] *Centre for Medical Radiation Physics, University of Wollongong, NSW, Australia*

Open Access Article. Published on 08 February 2024. Downloaded on 1/11/2026 3:15:51 AM.
This article is licensed under a Creative Commons Attribution 3.0 Unported Licence.

it takes part in fundamental processes, including its alkylation with ethylene to obtain ethylbenzene, which feeds the production of styrene monomers.[3] Although many theoretical and experimental electron scattering studies have been conducted on gaseous benzene[4–8] (and references therein), the results available in the condensed phase are somewhat scarce. It is interesting to note that previous studies on electron interactions with benzene clusters[9–11] may help to understand the nature and evolution of condensation effects. In particular, Pysanenko[12] *et al.* showed that $C_6H_6^-$ anion, which is unstable in the gas phase and produced by electron attachment, is stabilized in a cluster environment by opening the ring to release the internal energy.

The adsorption of benzene on different transition metal surfaces, like platinum (Pt), has been comprehensively studied from both experimental and theoretical approaches. Over the years, different techniques have been used to characterize the benzene/Pt system which includes angle resolved ultraviolet photoelectron spectroscopy (ARUPS),[13] low energy electron diffraction (LEED),[14,15] electron energy loss spectroscopy (EEL)[16] and high-resolution EEL,[17–19] near edge X-ray absorption fine structure (NEXAFS),[20] temperature programmed desorption (TPD),[21,22] reflection absorption IR spectroscopy (RAIRs),[23] surface enhanced Raman spectroscopy (SERS)[24] and scanning tunneling microscopy (STM).[25–27] Calculations have been performed within the framework of density functional theory (DFT),[28–35] semiempirical atom superposition, electron delocalization molecular orbital (ASED-MO) theory[36,37] and a variety of other *ab initio* computations to study the interaction of benzene with platinum clusters.[38] The reactivity of platinum cluster ions with benzene has also been experimentally studied by Liu *et al.*[39]

A study of ESD yielding cations from physisorbed benzene both directly on a Pt surface and on a 15ML argon spacer layer was performed by Kawanowa *et al.*[40] back in 2003. Although these authors could observe the cation ESD yield from the benzene molecule adsorbed on the argon spacer layer, the low sensitivity of the experimental setup prevented the detection of any other desorbed fragments, apart from H^+ after benzene deposited directly on the Pt surface. Many of the main experimental contributions to ESD from biomolecules of relevant radiobiological interest such as thiophene,[41] nitromethane,[42,43] NO and N_2O[44] and DNA,[45–47] have been performed in our laboratory at the University of Sherbrooke using the experimental set up employed in the present study.

The dissociation processes involved in the ESD of anionic and cationic fragments are predominantly dissociative electron attachment (DEA), dipolar dissociation (DD) and dissociative ionization (DI). In DEA, the incoming electron is resonantly captured by the molecule (M) to form a transient negative ion (TNI), M^{*-} which may dissociate into an anionic and one or more neutral fragments, *e.g.*

$$e^- + M \rightarrow M^{*-} \rightarrow A^- + B. \quad (1)$$

This process competes with the alternative electron autodetachment decay channel, *i.e.*,

$$M^{*-} \rightarrow e^- + M^*. \quad (2)$$

As the DEA process is mediated by resonant electron capture, its energy dependence below 20 eV consists of peaked structures, the shapes of which are determined by the lifetime of the relevant TNI and the potential energy surface involved which in turn are sensitive to the molecular electronic structure. Therefore, DEA anion yields obtained in the condensed phase may show some differences from those obtained in the gas phase.[48,49]

In contrast, DD occurs when the neutral molecule, once electronically excited by the incoming electron, dissociates into a pair of oppositely charged fragments, *i.e.*,

$$e^- + M \rightarrow M^* + e^- \rightarrow A^+ + B^- + e^-. \quad (3)$$

This is usually a non-resonant process resulting from direct electronic excitation of specific electronically excited dissociation states of the target molecule. Hence, its energy dependence is characterized by a threshold, which is usually slightly above the ionization of the intact molecule, followed by a monotonic increase.[50–52]

Finally, DI consists of the dissociation of the parent cation formed after ionization from the incoming electron,[53]

$$e^- + M \rightarrow M^{*+} + 2e^- \rightarrow A^+ + B + 2e^- \quad (4)$$

Here, we investigate ESD processes in thin films of benzene of different thicknesses deposited on a Pt substrate, by recording the yield of positively and negatively charged fragment ions as a function of the electron impact energy. The information gained from these studies is relevant to assess the electronic state spectroscopy of condensed molecular targets.

The remaining structure of this paper is as follows. In Section 2, we describe the experimental techniques. The results of ESD of cations and anions are presented in Section 3. A discussion of these results, as well as the likely fragmentation processes involved, is described in Section 4. Finally, conclusions drawn from the present work are presented.

Experimental

The ESD yields of ions were measured at the University of Sherbrooke (Canada). The experimental set up has been described in detail in previous publications.[41,54] In brief, the ESD apparatus comprises a Kimball Physics ELG-2 electron gun placed at 45° with respect to the target substrate normal axis. The electron gun operates in the pulsed mode, with a pulse duration of 800 ns at a frequency of 5 kHz. The electron beam is focused into a spot size of 3 mm in diameter. With appropriate refocusing, the electron gun can produce an electron beam from approximately 10 eV to 1 keV, with a time-averaged current of about 6 nA. Films of benzene are deposited directly on a polycrystalline Pt foil mounted on a closed cycle He cryostat that allows substrate temperatures to be controlled between 20 and 300 K. Before benzene deposition, the surface is cleaned by multiple resistive heating cycles at ≈1000 K. Films are formed from benzene vapor that emanate from the tip of a stainless-steel capillary tube, that is placed at ≈1 cm from the Pt foil, also at 45° to the surface normal. Vapor enters

 This journal is © the Owner Societies 2024

Open Access Article. Published on 08 February 2024. Downloaded on 1/11/2026 3:15:51 AM.
This article is licensed under a Creative Commons Attribution 3.0 Unported Licence.

the capillarity *via* an all-metal leak valve, from a small, turbo-pumped manifold, in which the absolute vapor pressure is monitored by a capacitance manometer. The system is calibrated such that the change in pressure corresponding to the formation of 1ML is known.[55] Film thicknesses are thus determined within an accuracy of about ±30% and an overall repeatability of ±0.2ML. For this study, the incident electron energy was varied between 10 and 950 eV and the layer thickness from 0.5 to 12ML. Each experimental measurement consisted of 10 runs of 20 seconds with an estimated time resolution of 2 ns. Ions desorbed from the samples during electron bombardment were directed into a time-of-flight mass analyzer (TOF-MS), positioned along the surface normal at 10 mm from the sample. TOF measurements were initiated by applying a voltage pulse of 2 kV (positive or negative for cations and anions detection, respectively) to the Pt surface, 10 ns after each electron pulse. Anions and cations were investigated in separate experiments. Between each experiment, sample films were removed from the Pt by resistive heating and a fresh film was deposited. All the measurements were performed under ultra-high vacuum conditions (*i.e.*, $\approx 2 \times 10^{-10}$ torr).

Results

Anion desorption yield

In Fig. 1, we show the results of the anionic ESD fragment yields grouped by the number of carbon atoms. These results were obtained for a fixed irradiation energy of 950 eV and different thicknesses varying from 0.5 to 8ML of the benzene film (top), and for different irradiation energies (from 10 to 950 eV) and 2 monolayers (ML) of benzene deposited on a Pt(111) substrate (bottom).

The anion yields qualitatively show a similar energy dependence for all fragments. At electron impact energies below 100 eV, desorption yields increase rapidly with increasing energy, while between 100 and 500 eV, the yields are fairly constant. Above 500 eV and up to 950 eV, a decrease in desorption yields is observed for all fragments. Regarding the thickness dependence, most of the anion yields attain their respective maximal intensity at 2ML and then decrease at a rate which is higher for heavier fragments, while the H^- yield remains constant and that for CH_n^- increases slightly for thicker benzene films.

The most intense fragment anion over the entire electron energy region is H^-, which is not unexpected given its lighter mass, and in general, desorption yields decrease as fragment anions are becoming heavier, *e.g.*, the yield of $H^- > CH_n^- \gg C_5H_n^-$. One interesting aspect of the fragmentation pattern relates to the higher yields of anions containing even numbers of carbon atoms relative to those containing odd numbers, *i.e.*, the yield of $C_2H_n^- \gg CH_n^-$ and $C_4H_n^- \gg C_3H_n^-$, *etc.*

Additionally, anions heavier than the parent have also been detected and can be attributed to clusters and/or molecular anions produced in reactions with the fragments. These results are displayed in Fig. 2, where the most abundant are associated with 6 and 7 carbon atoms. As far as incident electron energy

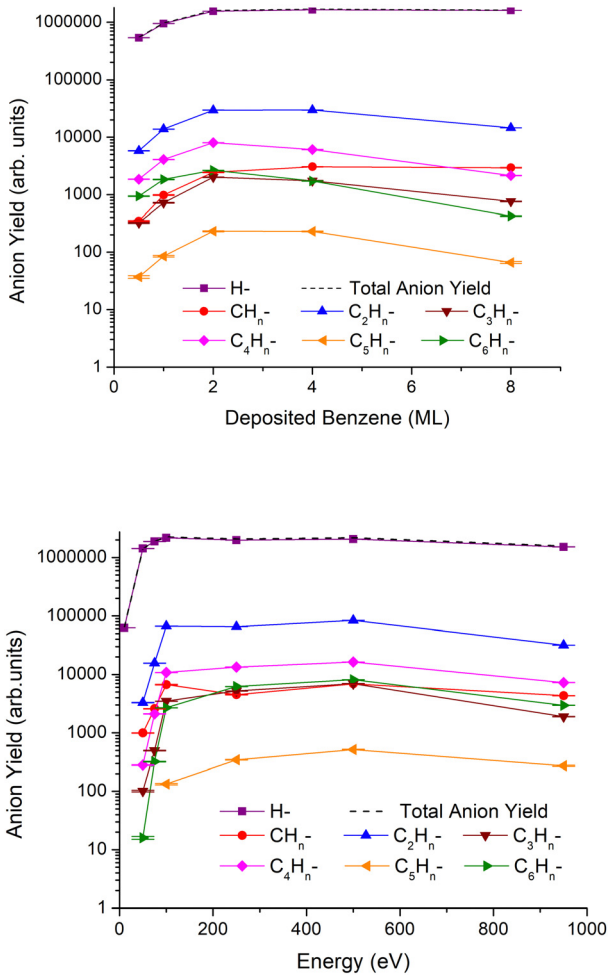

Fig. 1 (top) Electron stimulated desorption yields of anionic fragments for different thicknesses of benzene deposited on a Pt surface irradiated at an electron impact energy of 950 eV. (bottom) Electron stimulated desorption yields of anionic fragments from 2ML of benzene deposited on a Pt surface irradiated at different electron impact energies.

and thickness of the benzene layer are concerned, the maximum yields of heavier anions have been obtained for an irradiation energy of 500 eV and 4ML of deposited benzene.

Cation desorption yield

In Fig. 3, we show the results of cationic ESD fragment yields grouped by the number of carbon atoms as obtained for a fixed irradiation energy of 950 eV and different benzene thicknesses from 0.5 to 12ML (top), and for different irradiation energies and 2ML of benzene deposited on a Pt(111) substrate (bottom). The most intense cation is assigned to H^+, followed by other ions with increasing numbers of carbon atoms. If we compare the observed cation and anion yields as a function of the impact energy (see also Fig. 1, bottom), in both cases, the most intense fragment is the lightest (H^+ and H^-, respectively) and the intensities of the other fragments decrease with their respective masses. However, the decreasing intensity pattern for anions is different from that for cations. Note that for impact energies above 200 eV, in the case of anions, the decreasing tendency

Open Access Article. Published on 08 February 2024. Downloaded on 1/11/2026 3:15:51 AM.
This article is licensed under a Creative Commons Attribution 3.0 Unported Licence.

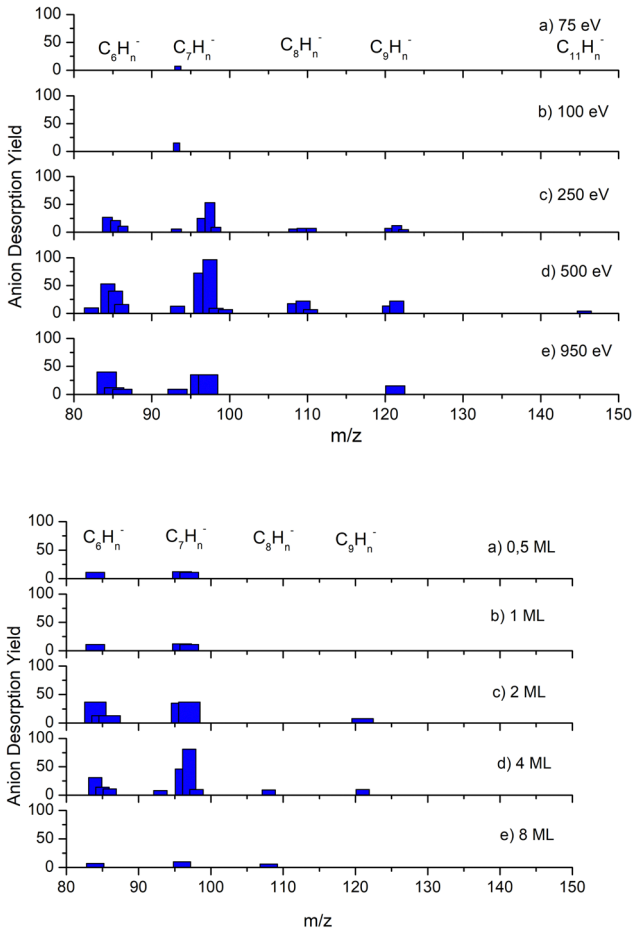

Fig. 2 (top) Anion desorption yield of clusters and/or molecular anions heavier than benzene from 2ML of benzene deposited on a Pt surface irradiated at different electron impact energies. (bottom) Anion desorption yield of different benzene layer thicknesses deposited on a Pt surface irradiated at 950 eV electron impact energy.

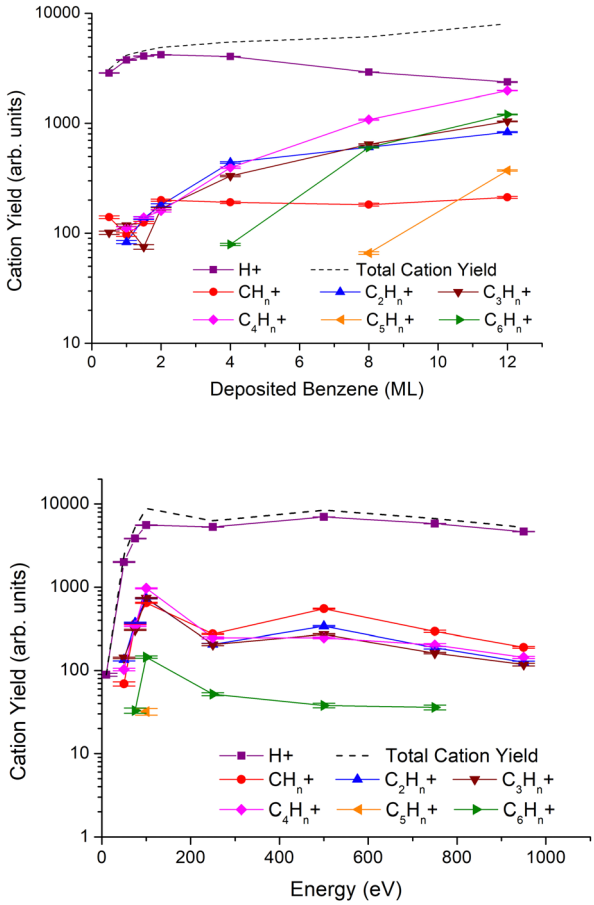

Fig. 3 (top) Cation desorption yield of different benzene layer thicknesses deposited on a Pt surface irradiated at 950 eV electron impact energy. (bottom) Cation desorption yield from 2ML of benzene deposited on a Pt surface irradiated at different electron impact energies.

with the mass of the fragments is altered for those with an even number of carbon atoms.

All cation yields peak at 100 eV and decrease up to 250 eV, although such a tendency is less pronounced in the case of H^+. Above 250 eV, the yields increase reaching a maximum at 500 eV, with the exception of $C_6H_n^+$, and monotonically decrease up to 900 eV. Fragment cations assigned to $C_5H_n^+$ are only observed at 100 eV. If we take this energy to be the maximum, the lack of any signal below and above such energy can be indicative of very low yields bearably discernible from the background signal. Yet, it is very interesting to observe the operative mechanism at the surface that quenches these cations' formation; these could be related to either geometrical effects or energy constraints limiting their effective desorption.

Regarding the benzene layer thicknesses on the ion yields dependence, H^+ shows a maximum for 2ML, and strongly decreases for thicker benzene films, while the yields of fragments containing at least 2 carbon atoms increase monotonically with film thickness. Note that in the case of CH_n^+, the maximum yield at 2ML remains constant regardless of the increase in the number of monolayers.

Discussion

As noted earlier, charged fragments desorbed in ESD experiments can be produced *via* DEA, DI and DD processes, which are discussed in the next sections.

Differences between gas- and condensed-phase

The cations' ESD mass spectrum from 75 eV electron impact energy on 2ML of benzene deposited on a platinum surface is shown in Fig. 4 together with the benzene gas-phase ionization mass spectrum from the NIST database[56] at 70 eV electron impact energy. Significant differences are observed between the condensed and the gas-phase results, indicating that different fragmentation processes and/or post-dissociation interactions occur in each phase.[40,57] Most of the cationic species formed in the gas-phase are observed in the condensed-phase but with differences in their associated relative intensities. The parent cation is found to be the most intense in the gas-phase, while in the condensed-phase, it is the lightest fragment cation, H^+. We also note in ESD experiments complete depletion of desorbed fragment cations assigned to $C_5H_n^+$. The prominence of lighter fragments such as H^+, CH_n^+, $C_2H_n^+$, $C_3H_n^+$ in ESD can be related

Open Access Article. Published on 08 February 2024. Downloaded on 1/11/2026 3:15:51 AM.
This article is licensed under a Creative Commons Attribution 3.0 Unported Licence.

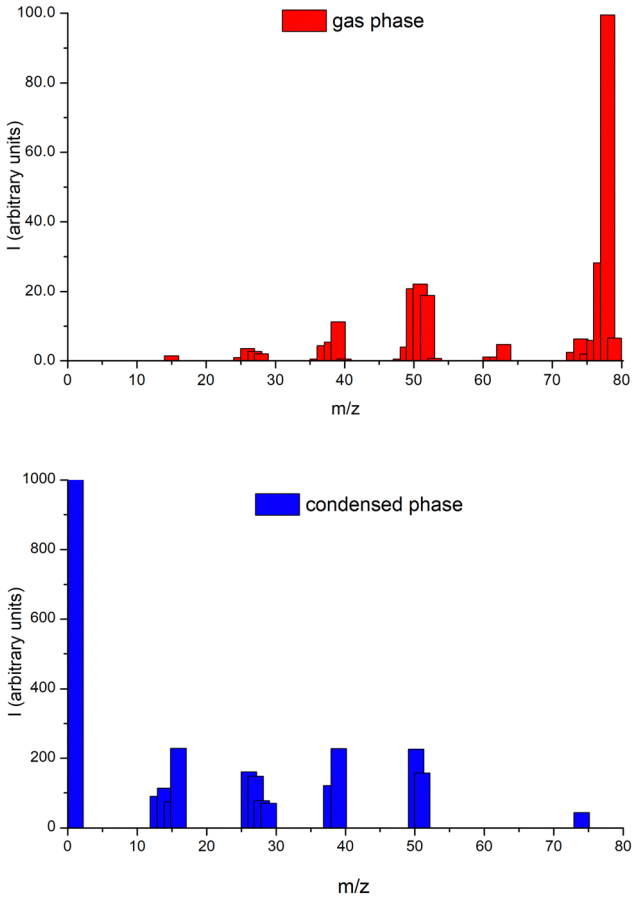

Fig. 4 Electron impact positive ion mass spectra from benzene. NIST gas phase data at 70 eV (top) and condensed phase ESD results for two monolayers of benzene on platinum surface irradiated at 75 eV (bottom).

to their high initial kinetic energy arising from dissociation on steep potential energy surfaces, which favors their desorption from the benzene film. Considering that in the ionization process, most of the kinetic energy from momentum transfer is taken away by the electron, while the parent ion receives kinetic energy of the order of meV,[58] this energy is not sufficient to desorb the parent positive ion from the benzene film and is not expected to contribute substantially to the desorption of the heavier fragments, which share less of the dissociation kinetic energy than the lighter ones. Apart from ion–molecule collisions within the film, this latter consideration is mainly due to the attraction of image-charge potential created in the metal substrate, which favors the lighter fragments with higher kinetic energies. In this sense, it is also interesting to consider the desorption mechanism proposed by Antoniewicz[59] in which ions created with a lower probability to desorb from the film can, in a first step, be accelerated towards the metal by the image force. When sufficiently close to the metal substrate, they neutralize by electron transfer and are reflected back. Now, as neutral species, they are not subject to any image potential and so require much less kinetic energy to desorb. We are not able to detect such neutral fragments with the present experimental setup, but this mechanism may contribute to the observed lack of desorption of higher mass cationic fragments relative to their production in the gas-phase. A recent study from Zhou *et al.*[60] shows that a double ionization of one of the molecules of the benzene trimer producing one outer-valence and one inner-valence vacancies (30.0 eV threshold energy) can relax *via* ultrafast intermolecular decay mechanisms, leading to the formation of a benzene cluster trication which followed by a Coulomb explosion produces three $C_6H_6^+$ cations. This result reinforces the idea that the suppression of the parent cation in the condensed phase is directly related to the bulk properties of the target.

Energy dependence

The total anion and cation yields are depicted in Fig. 5 (top) for incident electron energies in the range 10–950 eV. The ratio between anionic and cationic species shows a strong energy dependence from 10 up to 250 eV, which can be attributed to the major role of DEA relative to DI processes, whereas above 250 eV such ratio is almost insensitive to the electron energy. This seems plausible since at these energies, the channel yielding DD is open. In fact, previous ESD experiments at lower energies in both the gaseous[52,61] and condensed[55,62–64] phases

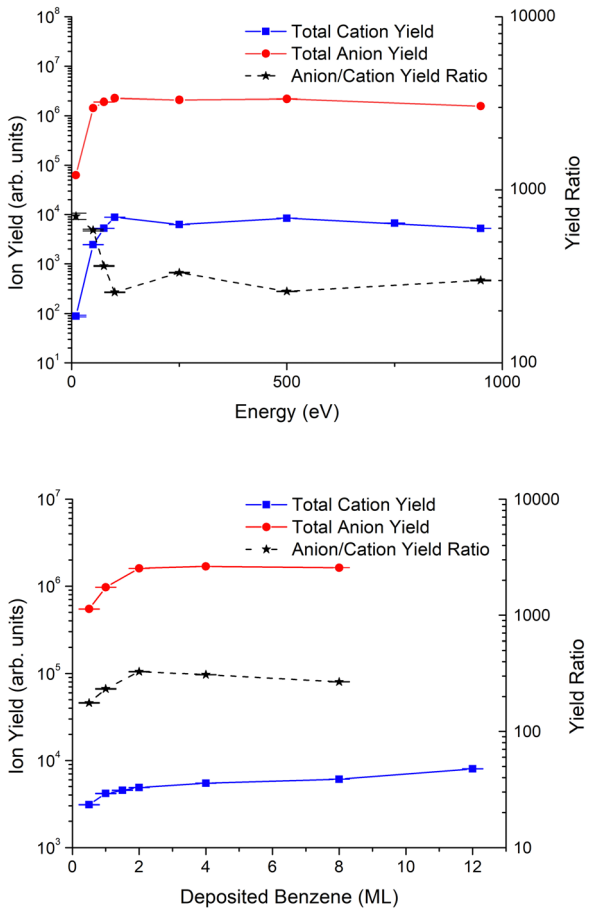

Fig. 5 Total anion and cation yields (left *y*-axis) and anion over cation yield rate (right *y*-axis) as a function of incident energy for a deposited benzene film of 2ML (top) and as a function of the benzene film thickness for a fixed incident energy of 950 eV (bottom).

Open Access Article. Published on 08 February 2024. Downloaded on 1/11/2026 3:15:51 AM. This article is licensed under a Creative Commons Attribution 3.0 Unported Licence.

have generally shown that the typical contribution of DD shows a monotonic increase above the ionization energy which tends to reach a plateau for higher energies.

Benzene film thickness dependence

Fig. 5 (bottom) shows the total anion and cation yields as a function of benzene thickness. A close inspection of the figure indicates that the anion yield increases rapidly up to a thickness of 2ML and then remains constant for thicker benzene films. In contrast, the cation yield increases quasi-monotonically for films of up to 12ML of benzene.

The anion yield behaviour is in good agreement with the model applied previously by Sanche and co-workers[64,65] to low energy electron stimulated desorption of light anionic fragments from biomolecules, such as thymine, uracil and 5-halouracil. According to this model, saturation is achieved due to the combined effect of a longer path through benzene increasing the interaction probability of the electrons, and the smaller desorption probabilities of the fragments created in deeper layers of the deposited film. This justifies that the H^- yield remains almost constant for film thickness >2ML. However, the monotonous increase in cation yield with thickness suggests a corresponding enhancement in the cation production probability at larger distances from the metal substrate. The metal effects in fragmentation and desorption of ions that have been previously discussed[66–69] are mainly associated with the image-charge potential induced by the metal and the corresponding polarization energy. However, the presence of the metal influences not only the kinetic energy of the fragment ions, the dissociation branching and the configuration space,[61] but plays a major role in the desorption mechanism, by allowing secondary and tunneling electrons that can neutralize and reionize the fragments.[59] Due to this complex combination, a direct generalization from other experiments cannot be made to the net effect of the polycrystalline Pt substrate on the cation yield of ESD benzene films. Therefore, in order to get more conclusive results, further investigations of these specific metal effects will have to be performed by comparing similar measurements for benzene films with a rare gas-solid (RGS) buffer layer as discussed before for other molecules.[40,63,70,71]

Anion and cation yield magnitude

Despite the similarity of energy dependence, there is a large difference in magnitude between the cation and the anion yields from ESD experiments. For a fixed thickness of 2ML, the ratio of anion to cation yield is ≈700 at low energies and decreases to ≈300 for higher energies. Meanwhile, for a fixed impact energy of 950 eV, this ratio is about 200 for 0.5ML, increasing up to nearly 400 at 2ML and then slowly decreasing for higher thicknesses of the benzene film. By assuming a similar efficiency of our detector system for positive and negative charges, this difference in magnitude between anion and cation yields represents a major challenge to assert DD as the main fragmentation mechanism leading to anion ESD. Ideally, this mechanism should produce similar amounts of both negative and positive ions.

The initial dissociation dynamics of the fragmentation pathways during dipolar dissociation favour ESD of the lighter fragments, whose desorption probabilities are much higher than those of their associated heavier ones. So, the ratio of anion to cation ESD yields depends on the branching ratios between the mass of positive to that of negative fragments. According to our results, this branching ratio would produce more lighter anions. Furthermore, the thickness dependence observed in the anion/cation yield, which monotonically decreases above 2ML, may suggest that the difference is also due to an effect induced by the metal, which loses strength with increasing distance from it, *i.e.*, as further benzene monolayers are deposited, desorption from the outermost layer is favoured due to the shorter paths of the outgoing fragments. As recently noted by Omar *et al.*,[66] surface interactions between both the parent molecule and generated fragments can lead to their physisorption and even chemisorption on a clean Pt substrate. Such surface bonds are expected to reduce preferentially the yields of desorbed cations, which are generally more reactive than anions. Another metal effect enhancing dissociation pathways of lighter anionic fragments and affecting heavier cationic fragments has been reported by Antoniewicz.[59] According to this mechanism, the difference observed can be attributed to neutralization of cationic fragments by the abundant secondary electrons produced from both ionizations and secondary emissions from the metal substrate. Notwithstanding, we suggest that the observed difference must be the result of a complex combination of all these effects. In this sense, it is interesting to compare the present results with the dipolar desorption of H cations and anions from pyrimidine deposited over a 3ML argon buffer layer on a Pt substrate.[62] A significant difference in the magnitude of the anion and the cation yields was also observed at energies close to the DD threshold but the difference in magnitude was one order of magnitude smaller than that observed in the present study. In the pyrimidine ESD experiment, the argon buffer layer reduces any metal effects and limits the presence of secondary electrons emitted by the metal. Therefore, the presence of a still significant but much smaller difference might support our initial assumption, *i.e.*, the predominance of fragmentation pathways with lighter anionic fragments that is enhanced by the combination of metal image-charge effects, preferential surface bonding of cationic fragments and the abundance of secondary electrons.

Ion yield cross-section estimation and comparison with the literature

Assuming a perfect detection efficiency together with dipolar dissociation as the main production mechanism of desorbed charged fragments, it is possible to estimate the cross-section of the process from the total electron flux and the surface density of benzene molecules in the deposited film. The measured number, Y, of either positive or negative ions will be proportional to the electron flux, n_e, the exposure time, t, the dipolar dissociation cross-section, σ_{DD}, the desorption probability, P_{des}, and the surface molecular density of the deposited benzene film, ρ_{Bz}, as

$$Y = n_e \cdot t \cdot \sigma_{DD} \cdot P_{des} \cdot \rho_{Bz} \quad (5)$$

 This journal is © the Owner Societies 2024

Open Access Article. Published on 08 February 2024. Downloaded on 1/11/2026 3:15:51 AM.
This article is licensed under a Creative Commons Attribution 3.0 Unported Licence.

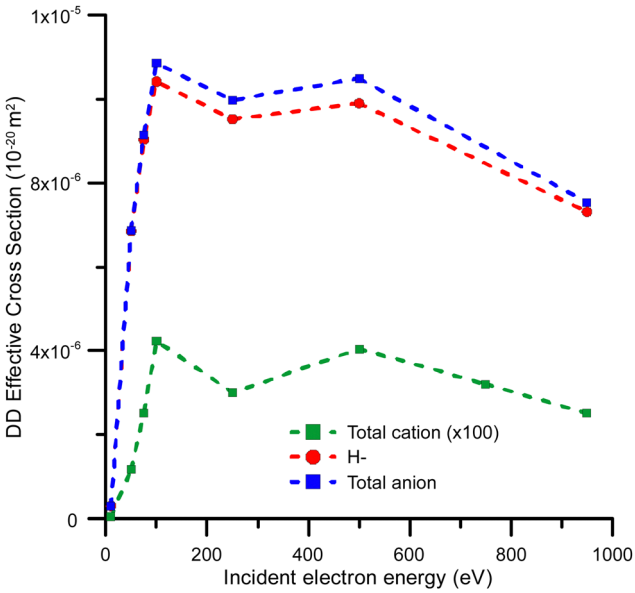

Fig. 6 Effective dipolar dissociation cross sections for total cation production (■), total anion production (■) and H anion production (●) by electron impact on 2ML of condensed benzene.

from which, we can obtain an effective cross-section, σ_{eff}, where the desorption probability is already accounted as

$$\sigma_{\mathrm{eff}} = \sigma_{\mathrm{DD}} \cdot P_{\mathrm{des}} = \frac{Y}{n_{\mathrm{e}} \cdot t \cdot \rho_{\mathrm{Bz}}} \tag{6}$$

where a mean beam intensity of 6 nA and a beam diameter of 3 mm deliver an electron flux of

$$n_{\mathrm{e}} = 5.2984 \times 10^{15} \text{ electrons per (s m}^2\text{)}, \tag{7}$$

the exposure times are given by the 10 runs of 20 seconds (t = 200 s) each during which the electron beam is operated at pulses with 800 ns duration at a frequency of 5 kHz and instantaneous current of 1.5 μA.

Besides, the molecular surface density has been estimated from the adsorption geometry of benzene over Pt to be

$$\rho_{\mathrm{Bz}} = 2.7812 \times 10^{18} \text{ molecules per m}^2. \tag{8}$$

The effective DD cross-section for total anion and cation production by electron impact on condensed benzene is shown in Fig. 6 together with that corresponding to H^- production. As far as authors are aware there are no published DD cross sections for benzene either in the gas or condensed phase to compare with the present results. Although the energy dependence of the present data can be considered reliable within the uncertainty limits discussed earlier, the absolute values shown in Fig. 6 are just an estimation which would require further validation.

The role of secondary electrons

The secondary electrons are produced either by ionization processes or by secondary emission from the metal[67,68] after irradiation by the primary electron beam impinging on the benzene film and traversing into the Pt substrate. As the kinetic energy of the secondary electrons is generally below 20 eV,[71–74] their effect with respect to charged fragment production should be mostly restricted to an increase in DEA interactions which would only manifest in a subsequent increase of the anion yields. Note that in the gas phase only $C_6H_5^-$ and $C_2H_2^-$ anion fragments are produced[75] and only $C_6H_6^-$ and $C_6H_5^-$ in the case of clusters.[12] However, neutralization of cationic fragments or the appearance of a charged lattice in the benzene film with the consequent influence in the desorption probabilities of charged fragments should also be considered in order to fully account for the observed cation and anion yields.

Heavier anions

Fragments heavier than the parent benzene molecule have been observed only for anions. These compounds can be attributed to clusters or molecular aggregates as a consequence of different reactions of one of the lightest negative fragments with benzene molecules or even of two intermediate mass fragments. Their total intensity is much lower than that of the other anion fragments. The lack of cations with heavier masses is not unexpected if we consider that the cation yields are about two orders of magnitude lower than those of the corresponding anions.

It is also interesting observed in Fig. 2 that the yield of such heavy anions, unlike those other lighter fragments, reaches its maximum at 500 eV. Additionally, we note that it is quite close to the expected maximum for secondary electron emission yield of the Pt substrate at ≈550 eV.[71] This suggests that secondary electrons may also play an important role in the ESD yield of these heavy anions, particularly if a dimer transient anion is formed. In this case, the decay channels include fragments that are heavier than the monomer, as shown by Sanche and Parenteau[74] and Sanche *et al.*[76] Although we are not able to provide any conclusive explanation, we suggest that, as their kinetic energy is expected to be quite low, the repulsive force between cations from a lattice positive charge built up in the film could favour their desorption.[77]

Conclusions

Novel ESD measurements of anion and cation yields from condensed benzene deposited on a Pt substrate have been investigated for a fixed film thickness of 2ML in the electron impact energy range of 10 to 950 eV. Moreover, we have also investigated anion and cation formation for a fixed impact energy of 950 eV for a range of thicknesses extending from 0.5ML to 12ML.

A qualitative similar behaviour was found in the energy dependence of anion and cation yields, where both show a monotonous increase up to ≈100 eV and a decrease up to 250 eV. Above 250 eV the yields increase reaching a maximum at 500 eV, except for $C_6H_n^+$, and monotonically decrease up to 900 eV. Their common qualitative behaviour and the monotonic increase from a threshold up to 100 eV suggested that DD could be the main initial mechanism.

Open Access Article. Published on 08 February 2024. Downloaded on 1/11/2026 3:15:51 AM.
This article is licensed under a Creative Commons Attribution 3.0 Unported Licence.

The thickness dependences of anions and cations ESD are significantly different. The anion yield reaches a plateau for thicknesses above 2ML, while the cation yield increases monotonically up to 12ML. Furthermore, the anion yield was found to be systematically larger than the cation yield by at least two orders of magnitude. Significant differences in the cation mass spectra were also observed between the ESD measurements and the NIST data for gaseous benzene. We have tentatively suggested that this could result from a complex interrelation between metal effects enhancing desorption of lighter fragments and dipolar dissociation pathways favouring lighter anionic fragments. In addition, we have also suggested that neutral fragment ESD measurements could support the Antoniewicz mechanism[59] in reducing the magnitude of cation yields compared to anions.

Another interesting aspect of the present investigation pertains to anions heavier than the benzene molecule to desorb from the films, which could arise from the formation of dimeric transient anions decaying *via* DEA into channels comprising fragments heavier than benzene. We have highlighted the role of the abundant secondary electrons emanating from the substrate in the heavy anion yield maximum at 500 eV.

Effective DD cross sections were also derived from ESD yields. These were compared with some of the data in the literature[52] corresponding to the DD yield of H^- anions from gaseous acetylene. A good level of agreement in both magnitude and behaviour has been found, which confidently supports our DD cross-section estimations.

Author contributions

Conceptualization and methodology, G. G. and L. S.; measurements, L. A. and A. D. B., data curation L. A., A. I. L. and A. G. A.; supervision A. D. B, P. L. V., G. G. and L. S.; original draft, A. G. A. and A. I. L.; review & editing, P. L. V., G. G., A. D. B. and L. S.

Conflicts of interest

There are no conflicts to declare.

Acknowledgements

This study has partially been supported by the Spanish Ministry of Science and Innovation (Project PID2019-104727RB-C21), A. G. A. and L. A. thank MICIU and the local CAM government, respectively, for their corresponding grants within the "Garantía Juvenil" programmes. A. I. L. and P. L. V. acknowledge the Portuguese National Funding Agency (FCT) through research Grants CEFITEC (UIDB/00068/2020). The experiments were supported by the Natural Science and Engineering Research Council of Canada (RGPIN-2018-14882).

Notes and references

1 G. García Gómez-Tejedor and M. C. Fuss, *Radiation Damage in Biomolecular Systems*, Springer Netherlands, 2012.
2 R. Nithyanandam, Y. K. Mun, T. S. Fong, T. C. Siew, O. S. Yee and N. Ismail, *J. Eng. Sci. Technol.*, 2018, **13**, 4290–4309.
3 H. You, W. Long and Y. Pan, The Mechanism and Kinetics for the Alkylation of Benzene with Ethylene, *Pet. Sci. Technol.*, 2006, **24**, 1079–1088.
4 F. Costa, L. Álvarez, A. I. Lozano, F. Blanco, J. C. Oller, A. Muñoz, A. S. Barbosa, M. H. F. Bettega, F. Ferreira da Silva, P. Limão-Vieira, R. D. White, M. J. Brunger and G. García, Experimental and theoretical analysis for total electron scattering cross sections of benzene, *J. Chem. Phys.*, 2019, **151**, 084310.
5 A. S. Barbosa and M. H. F. Bettega, Shape resonances, virtual state, and Ramsauer-Townsend minimum in the low-energy electron collisions with benzene, *J. Chem. Phys.*, 2017, **146**, 154302.
6 D. Prajapati, H. Yadav, P. C. Vinodkumar, C. Limbachiya, A. Dora and M. Vinodkumar, Computation of electron impact scattering studies on benzene, *Eur. Phys. J. D*, 2018, **72**, 210.
7 J. N. Bull, J. W. L. Lee and C. Vallance, Absolute electron total ionization cross-sections: molecular analogues of DNA and RNA nucleobase and sugar constituents, *Phys. Chem. Chem. Phys.*, 2014, **16**, 10743–10752.
8 A. I. Lozano, F. Costa, X. Ren, A. Dorn, L. Álvarez, F. Blanco, P. Limão-Vieira and G. García, Double and Triple Differential Cross Sections for Single Ionization of Benzene by Electron Impact, *Int. J. Mol. Sci.*, 2021, **22**, 4601.
9 A. Kiermeier, B. Ernstberger, H. J. Neusser and E. W. Schlag, Benzene clusters in a supersonic beam, *Z. Phys. D: At., Mol. Clusters*, 1988, **10**, 311–317.
10 A. Kiermeier, B. Ernstberger, H. J. Neusser and E. W. Schlag, Multiphoton Mass Spectrometry of Clusters: Dissociation Kinetics of the Benzene Cluster Ions, *J. Phys. Chem.*, 1988, **92**, 3785–3789.
11 M. Mitsui, A. Nakajima, K. Kaya and U. Even, Mass spectra and photoelectron spectroscopy of negatively charged benzene clusters, $(benzene)_n^-$ (n = 53–124), *J. Chem. Phys.*, 2001, **115**, 5707–5710.
12 A. Pysanenko, I. S. Vinklárek, J. Fedor, M. Fárník, S. Bergmeister, V. Kostal, T. Nemirovich and P. Jungwirth, Gas phase $C_6H_6^-$ anion: Electronic stabilization by opening of the benzene ring, *J. Chem. Phys.*, 2022, **157**, 224306.
13 M. Abon, J. C. Bertolini, J. Billy, J. Massardier and B. Tardy, Adsorption states of benzene and toluene on Pt(111): A vibrational EELS, Δφ, AES and TDS study, *Surf. Sci.*, 1985, **162**, 395–401.
14 J. Somers and T. Mccabe, An ARUPS investigation of benzene on Pt(111): evidence for distortion, *Surf. Sci.*, 1987, **181**, L167–L170.
15 J. L. Gland and G. A. Somorjai, Low energy electron diffraction and work function studies of benzene, naphthalene and pyridine adsorbed on Pt(111) and Pt(100) single crystal surfaces, *Surf. Sci.*, 1973, **38**, 157–186.
16 P. C. Stair and G. A. Somorjai, The adsorption of benzene on the Pt(111) surface studied by low-energy electron diffraction intensity measurements and quantitative Auger electron spectroscopy, *J. Chem. Phys.*, 1977, **67**, 4361–4369.

 This journal is © the Owner Societies 2024

Open Access Article. Published on 08 February 2024. Downloaded on 1/11/2026 3:15:51 AM.
This article is licensed under a Creative Commons Attribution 3.0 Unported Licence.

17 S. Lehwald, H. Ibach and J. E. Demuth, Vibration spectroscopy of benzene adsorbed on Pt(111) and Ni(111), *Surf. Sci.*, 1978, **78**, 577–590.
18 V. Demers-Carpentier and P. H. McBreen, Surface vibrational spectroscopy study of benzene and 2,2,2- trifluoroacetophenone on Pt(111), *J. Phys. Chem. C*, 2011, **115**, 6513–6520.
19 F. Cemic, O. Dippel and E. Hasselbrink, Resonant electron scattering from benzene chemisorbed on Pt(111), *Surf. Sci.*, 1995, **342**, 101–110.
20 J. A. Horsley, J. Stöhr, A. P. Hitchcock, D. C. Newbury, A. L. Johnson and F. Sette, Resonances in the K shell excitation spectra of benzene and pyridine: Gas phase, solid, and chemisorbed states, *J. Chem. Phys.*, 1985, **83**, 6099–6107.
21 J. Breitbach, D. Franke, G. Hamm, C. Becker and K. Wandelt, Adsorption of benzene on ordered Sn/Pt(1 1 1) surface alloys, *Surf. Sci.*, 2002, **507–510**, 18–22.
22 M.-C. Tsai and E. L. Muetterties, Platinum Metal Surface Chemistry of Benzene and Toluene, *J. Am. Chem. Soc.*, 1982, **104**, 2534–2539.
23 S. Haq and D. A. King, Configurational transitions of benzene and pyridine adsorbed on Pt{111} and Cu{110} surfaces: An infrared study, *J. Phys. Chem.*, 1996, **100**, 16957–16965.
24 G. K. Liu, B. Ren, D. Y. Wu, S. Duan, J. F. Li, J. L. Yao, R. A. Gu and Z. Q. Tian, Effect of intrinsic properties of metals on the adsorption behavior of molecules: Benzene adsorption on Pt group metals, *J. Phys. Chem. B*, 2006, **110**, 17498–17506.
25 P. S. Weiss and D. M. Eigler, Site dependence of the apparent shape of a molecule in scanning tunneling micoscope images: Benzene on Pt{111}, *Phys. Rev. Lett.*, 1993, **71**, 3139–3142.
26 D. N. Futaba and S. Chiang, Calculations of scanning tunneling microscopic images of benzene on Pt(111) and Pd(111), and thiophene on Pd(111), *Jpn. J. Appl. Phys., Part 1*, 1999, **38**, 3809–3812.
27 P. Sautet and M. Bocquet, Shape of molecular adsorbates in STM images: A theoretical study of benzene on Pt(111), *Phys. Rev. B: Condens. Matter Mater. Phys.*, 1996, **53**, 4910–4925.
28 C. Morin, D. Simon and P. Sautet, Intermediates in the hydrogenation of benzene to cyclohexene on Pt(1 1 1) and Pd(1 1 1): A comparison from DFT calculations, *Surf. Sci.*, 2006, **600**, 1339–1350.
29 W. Gao, W. T. Zheng and Q. Jiang, Dehydrogenation of benzene on Pt(111) surface, *J. Chem. Phys.*, 2008, **129**, 1–9.
30 K. G. Lakshmikanth, P. K. Ayishabi and R. Chatanathodi, Ab initio DFT studies of adsorption characteristics of benzene on close-packed surfaces of transition metals, *Comput. Mater. Sci.*, 2017, **137**, 10–19.
31 C. Morin, D. Simon and P. Sautet, Chemisorption of Benzene on Pt(111), Pd(111), and Rh(111) Metal Surfaces: A Structural and Vibrational Comparison from First Principles, *J. Phys. Chem. B*, 2004, **108**, 5653–5665.
32 M. Saeys, M.-F. Reyniers, G. B. Marin and M. Neurock, Density functional study of benzene adsorption on Pt(111), *J. Phys. Chem. B*, 2002, **106**, 7489–7498.
33 W. Liu, J. Carrasco, B. Santra, A. Michaelides, M. Scheffler and A. Tkatchenko, Benzene adsorbed on metals: Concerted effect of covalency and van der Waals bonding, *Phys. Rev. B: Condens. Matter Mater. Phys.*, 2012, **86**, 1–6.
34 F. Mittendorfer, C. Thomazeau, P. Raybaud and H. Toulhoat, Adsorption of unsaturated hydrocarbons on Pd(111) and Pt(111): A DFT study, *J. Phys. Chem. B*, 2003, **107**, 12287–12295.
35 W. Liu, V. G. Ruiz, G. X. Zhang, B. Santra, X. Ren, M. Scheffler and A. Tkatchenko, Structure and energetics of benzene adsorbed on transition-metal surfaces: Density-functional theory with van der Waals interactions including collective substrate response, *New J. Phys.*, 2013, **15**, 053046.
36 A. B. Anderson, M. R. McDevitt and F. L. Urbach, Structure and electronic factors in benzene coordination to $Cr(CO)_3$ and to cluster models of Ni, Pt, and Ag (111) surfaces, *Surf. Sci.*, 1984, **146**, 80–92.
37 C. Minot, Benzene Adsorption on Pt(111): a theoretical study, *Surf. Rev. Lett.*, 1995, **2**, 285–295.
38 D. Majumdar, S. Roszak and K. Balasubramanian, Interaction of benzene (Bz) with Pt and Pt2: A theoretical study on Bz-Pt2, Bz2-Pt, Bz2-Pt2, and Bz3-Pt2 clusters, *J. Chem. Phys.*, 2001, **114**, 10300.
39 H. Liu, S. Sun, X. Xing and Z. Tang, Reactions of platinum cluster ions with benzene, *Rapid Commun. Mass Spectrom.*, 2006, **20**, 1899–1904.
40 H. Kawanowa, M. Kondo, K. Hanatani, Y. Gotoh and R. Souda, Electron stimulated desorption of cations from C6H6 and C6H12 molecules adsorbed on Pt(111) and Ar spacer layer, *Nucl. Instrum. Methods Phys. Res. Sect., B: Beam Interact. Mater. Atoms*, 2003, **203**, 178–182.
41 M. N. Hedhili, P. Cloutier, A. D. Bass, T. E. Madey and L. Sanche, Electron stimulated desorption of anionic fragments from films of pure and electron-irradiated thiophene, *J. Chem. Phys.*, 2006, **125**, 1–12.
42 M. Bazin, S. Ptasińska, A. D. Bass and L. Sanche, Electron induced dissociation in condensed-phase nitromethane I: desorption of ionic fragments, *Phys. Chem. Chem. Phys.*, 2009, **11**, 1610–1618.
43 M. Bazin, S. Ptasinska, A. D. Bass, L. Sanche, E. Burean and P. Swiderek, Electron induced dissociation in the condensed-phase nitromethane: II. Desorption of neutral fragments, *J. Phys.: Condens. Matter*, 2010, **22**, 084003.
44 L. Sanche and L. Parenteau, Dissociative attachment in electron-stimulated desorption from condensed NO and N 2 O, *J. Vac. Sci. Technol., A*, 1986, **4**, 1240–1242.
45 H. Abdoul-Carime, P. Cloutier and L. Sanche, Low energy (5-40eV) electron stimulated desorption of Anions from Desorption DNA Bases Physisorbed, *Radiat. Res.*, 2001, **155**, 625–633.
46 M. A. Hervé du Penhoat, M. A. Huels, P. Cloutier, J. P. Jay-Gerin and L. Sanche, Electron stimulated desorption of H- from thin films of 5-halouracils, *Phys. Chem. Chem. Phys.*, 2003, **233**, 3270–3277.
47 E. Alizadeh, S. Massey, L. Sanche and P. A. Rowntree, Low-energy Electrons Interactions with Chemisorbed and Physisorbed Films of L-cysteine/Au(111), *J. Phys.: Conf. Ser.*, 2015, **635**, 062008.
48 O. Ingólfsson, F. Weik and E. Illenberger, The reactivity of slow electrons with molecules at different degrees of

Open Access Article. Published on 08 February 2024. Downloaded on 1/11/2026 3:15:51 AM.
This article is licensed under a Creative Commons Attribution 3.0 Unported Licence.

aggregation: gas phase, clusters and condensed phase, *Int. J. Mass Spectrom. Ion Processes*, 1996, **155**, 1–68.
49 P. Możejko, A. D. Bass, L. Parenteau and L. Sanche, Intrinsic and extrinsic factors in anion electron-stimulated desorption: D− from deuterated hydrocarbons condensed on Kr and water ice films, *J. Chem. Phys.*, 2004, **121**, 10181–10189.
50 L. Parenteau, J.-P. Jay-Gerin and L. Sanche, Electron-Stimulated Desorption of H- Ions via Dissociative Electron Attachment in Condensed Methanol, *J. Phys. Chem.*, 1994, **98**, 10277–10281.
51 C. R. Arumainayagam, H.-L. Lee, R. B. Nelson, D. R. Haines and R. P. Gunawardane, Low-energy electron-induced reactions in condensed matter, *Surf. Sci. Rep.*, 2010, **65**, 1–44.
52 E. Szymańska, I. Čadež, E. Krishnakumar and N. J. Mason, Electron impact induced anion production in acetylene, *Phys. Chem. Chem. Phys.*, 2014, **16**, 3425–3432.
53 E. Böhler, J. Warneke and P. Swiderek, Control of chemical reactions and synthesis by low-energy electrons, *Chem. Soc. Rev.*, 2013, **42**, 9219.
54 M. Bazin, S. Ptasińska, A. D. Bass and L. Sanche, Electron induced dissociation in condensed-phase nitromethane I: desorption of ionic fragments, *Phys. Chem. Chem. Phys.*, 2009, **11**, 1610.
55 L. Sanche, Transmission of 0-15 eV monoenergetic electrons through thin-film molecular solids, *J. Chem. Phys.*, 1979, **71**, 4860–4882.
56 W. E. Wallace, Mass Spectra in NIST Chem. Webb., NIST Stand, *Ref. Database*, 2023, **69**, DOI: **10.18434/T4D303**.
57 F. D. A. Ribeiro, B. Rudek, H. B. A. Cerqueira, R. R. Oliveira, A. B. Rocha, M. L. M. Rocco and W. Wolff, Fragment and cluster ions from gaseous and condensed pyridine produced under electron impact, *Phys. Chem. Chem. Phys.*, 2018, **20**, 25762–25771.
58 X. Wang, Z. Chen, B. Wei, R. Hutton and Y. Zou, Kinetic energy distribution for the ionization and dissociation process of C 2 H 4 by electron impact, *J. Phys. Conf. Ser.*, 2015, **576**, 012011.
59 P. R. Antoniewicz, Model for electron- and photon-stimulated desorption, *Phys. Rev. B: Condens. Matter Mater. Phys.*, 1980, **21**, 3811–3815.
60 J. Zhou, X. Yu, S. Luo, X. Xue, S. Jia, X. Zhang, Y. Zhao, X. Hao, L. He, C. Wang, D. Ding and X. Ren, *Nat. Commun.*, 2022, **13**, 5335.
61 D. Chakraborty, P. Nag and D. Nandi, Dipolar dissociation dynamics in electron collisions with carbon monoxide, *Phys. Chem. Chem. Phys.*, 2016, **18**, 32973–32980.
62 E. Alizadeh, S. Massey, L. Sanche and P. A. Rowntree, Low-energy electron-induced dissociation in condensed-phase L-cysteine II: a comparative study on anion desorption from chemisorbed and physisorbed films, *Eur. Phys. J. D*, 2016, **70**, 75.
63 L. Ellis-Gibbings, A. D. Bass, P. Cloutier, G. García and L. Sanche, Electron stimulated desorption from condensed pyrimidine and pyridazine, *Phys. Chem. Chem. Phys.*, 2017, **19**, 13038–13048.
64 M.-A. Hervé du Penhoat, M. A. Huels, P. Cloutier, J.-P. Jay-Gerin and L. Sanche, Electron stimulated desorption of H− from thin films of thymine and uracil, *J. Chem. Phys.*, 2001, **114**, 5755–5764.
65 M.-A. Hervé du Penhoat, M. A. Huels, P. Cloutier, J.-P. Jay-Gerin and L. Sanche, Electron stimulated desorption of H − from thin films of 5-halouracils, *Phys. Chem. Chem. Phys.*, 2003, **5**, 3270–3277.
66 H. Sambe, D. E. Ramaker, L. Parenteau and L. Sanche, Image charge effects in electron stimulated desorption: 0- from 02 Condensed on Ar Films Grown on Pt, *Phys. Rev. Lett.*, 1987, **59**, 236–239.
67 H. Chen, Y. Chen, A. Aleksandrov, J. Dong, M. Liu and T. M. Orlando, Charging effects on electron-stimulated desorption of cations from gadolinia-doped ceria surfaces, *Appl. Surf. Sci.*, 2005, **243**, 166–177.
68 P. Rowntree, L. Parenteau and L. Sanche, Anion yields produced by low-energy electron impact on condensed hydrocarbon films, *J. Phys. Chem.*, 1991, **95**, 4902–4909.
69 D. Antic, L. Parenteau and L. Sanche, Electron-Stimulated Desorption of H - from Condensed-Phase Deoxyribose Analogues: Dissociative Electron Attachment versus Resonance Decay into Dipolar Dissociation, *J. Phys. Chem. B*, 2000, **104**, 4711–4716.
70 P. Swiderek, M. Michaud and L. Sanche, Electron-energy-loss spectroscopy of 6,6′-dimethylfulvene: First detection of the triplet state, *J. Chem. Phys.*, 1998, **103**, 8424.
71 Y. Lin and D. C. Joy, A new examination of secondary electron yield data, *Surf. Interface Anal.*, 2005, **37**, 895–900.
72 N. Omar, P. Cloutier, C. Ramseyer, L. Sanche and M. Fromm, The role of repulsive and attractive forces in low-energy (3–15 eV) electron stimulated desorption of anions from molecular layers grown on clean and contaminated metallic substrates, *Chem. Phys.*, 2023, **564**, 111661.
73 N. Bundaleski, M. Belhaj, T. Gineste and O. M. N. D. Teodoro, *2013 IEEE 14th International Vacuum Electronics Conference (IVEC)*, IEEE, 2013, pp. 1–2.
74 L. Sanche and L. Parentau, Production of anion-atom complexes by electron stimulated desorption, *J. Chem. Phys.*, 1989, **90**, 3402–3403.
75 H.-P. Fenzlaff and E. Illenberger, Loe energy electron impact on benzene and the fluorobenzenes. Formation and dissociation of negative ions, *Int. J. Mass Spectrom. Ion Processes*, 1984, **59**, 185–202.
76 L. Sanche, L. Parenteau and P. Cloutier, Dissociative attachment reactions in electron stimulated desorption from condensed O_2 and O_2-doped rare-gas matrices, *J. Chem. Phys.*, 1989, **91**, 2664–2674.
77 Y. Dong, H. Liao, Y. Gao, P. Cloutier, Y. Zheng and L. Sanche, Early Events in Radiobiology: Isolated and Cluster DNA Damage Induced by Initial Cations and Nonionizing Secondary Electrons, *J. Phys. Chem. Lett.*, 2021, **12**, 717–723.

 This journal is © the Owner Societies 2024